Hot Carrier Generation and Extraction of Plasmonic Alloy Nanoparticles

Valenti, Marco; Venugopal, Anirudh; Tordera, Daniel; Jonsson, Magnus P.; Biskos, George; Schmidt-Ott, Andreas; Smith, Wilson A.

DOI
10.1021/acsphotonics.6b01048

Publication date
2017

Document Version
Final published version

Published in
ACS Photonics

ACS Photonics

Article

pubs.acs.org/journal/apchd5

Hot Carrier Generation and Extraction of Plasmonic Alloy Nanoparticles

Marco Valenti,*[,†] Anirudh Venugopal,[†] Daniel Tordera,[‡] Magnus P. Jonsson,[‡] George Biskos,[§,∥] Andreas Schmidt-Ott,[†] and Wilson A. Smith*[,†]

[†]Materials for Energy Conversion and Storage (MECS), Department of Chemical Engineering, Faculty of Applied Sciences, Delft University of Technology, Delft 2628-BL, The Netherlands

[‡]Laboratory of Organic Electronics, Department of Science and Technology, Campus Norrköping, Linköping University, SE-60174 Norrköping, Sweden

[§]Faculty of Civil Engineering and Geosciences, Delft University of Technology, Delft 2628-CN, The Netherlands

[∥]Energy Environment and Water Research Center, The Cyprus Institute, Nicosia 2121, Cyprus

Supporting Information

ABSTRACT: The conversion of light to electrical and chemical energy has the potential to provide meaningful advances to many aspects of daily life, including the production of energy, water purification, and optical sensing. Recently, plasmonic nanoparticles (PNPs) have been increasingly used in artificial photosynthesis (e.g., water splitting) devices in order to extend the visible light utilization of semiconductors to light energies below their band gap. These nanoparticles absorb light and produce hot electrons and holes that can drive artificial photosynthesis reactions. For n-type semiconductor photoanodes decorated with PNPs, hot charge carriers are separated by a process called hot electron injection (HEI), where hot electrons with sufficient energy are transferred to the conduction band of the semiconductor. An important parameter that affects the HEI efficiency is the nanoparticle composition, since the hot electron energy is sensitive to the electronic band structure of the metal. Alloy PNPs are of particular importance for semiconductor/PNPs composites, because by changing the alloy composition their absorption spectra can be tuned to accurately extend the light absorption of the semiconductor. This work experimentally compares the HEI efficiency from Ag, Au, and Ag/Au alloy nanoparticles to TiO_2 photoanodes for the photoproduction of hydrogen. Alloy PNPs not only exhibit tunable absorption but can also improve the stability and electronic and catalytic properties of the pure metal PNPs. In this work, we find that the Ag/Au alloy PNPs extend the stability of Ag in water to larger applied potentials while, at the same time, increasing the interband threshold energy of Au. This increasing of the interband energy of Au suppresses the visible-light-induced interband excitations, favoring intraband excitations that result in higher hot electron energies and HEI efficiencies.

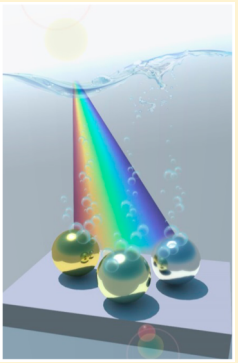

KEYWORDS: *hot electron injection, alloy nanoparticles, plasmonic nanoparticles, artificial photosynthesis, hydrogen photoproduction, gold nanoparticles, silver nanoparticles*

Photoelectrochemical (PEC) water splitting is a promising approach to produce hydrogen as a sustainable fuel from abundant resources.[1,2] In a PEC water splitting cell based on a single photoelectrode, semiconductors are used to absorb light and generate charge carriers (electron−hole pairs), which are subsequently separated to carry out the oxygen and hydrogen evolution reactions on the semiconductor surface and corresponding metal counter electrode. N-type metal oxide semiconductors have been extensively investigated as water splitting photoanodes due to their excellent stability in aqueous solutions and their ability to catalyze the oxygen evolution half-reaction.[2] However, an important limitation of metal oxide semiconductors is their poor visible light absorption due to their relatively large band gaps. Decorating metal oxide semiconductors with plasmonic nanoparticles (PNPs) that absorb visible light can extend the hydrogen generation of metal oxide water splitting devices to light energies below the semiconductor *optical* band gap edge (OBGE).[3] These metallic PNPs are characterized by the light-induced collective oscillation of their free electrons (surface plasmons). The below OBGE light harvesting ability of the decorating PNPs has been explained by two mechanisms: (i) hot electron injection (HEI)[3] and (ii) plasmon-induced resonance energy transfer (PIRET).[4] HEI (i) is the process in which plasmon-induced hot electrons (electrons with energies higher than the metal Fermi level) in the metallic PNPs are transferred to the conduction band of a contacting semiconductor. In the case of a semiconductor photoanode, the hot electron transferred to the conduction band migrates to the metal counter electrode (e.g., Pt) to evolve hydrogen. The "hot" hole, left behind in the metal PNP, can be extracted with an electron acceptor catalyst to evolve oxygen[3] or by adding a sacrificial agent in the electrolyte.[5] PIRET (ii), on the other hand, is a mechanism in

Received: January 3, 2017
Published: March 6, 2017

DOI: 10.1021/acsphotonics.6b01048
ACS Photonics 2017, 4, 1146−1152

which the surface plasmon decays by inducing electron hole pairs directly in the semiconductor through a dipole−dipole interaction with a transient exciton.[6] One important advantage of the HEI mechanisms is that, unlike PIRET, its efficiency does not depend on the semiconductor's absorption band edge,[4] allowing the ability to extend the light utilization of the device to even longer wavelengths (e.g., near-infrared). However, the efficiency of the HEI mechanism is significantly limited since the plasmon-induced hot electrons/hot holes need to efficiently undergo several processes: (i) the charges need to reach the surface of the PNP, (ii) the hot electrons must have sufficient energy, above the metal Fermi level, to cross the metal/semiconductor Schottky energy barrier, and (iii) the hot holes need to be efficiently extracted to continuously maintain charge neutrality in the metal PNP upon the HEI process.[7] Due to the poor overall efficiency of these processes, most of the plasmon-induced hot electrons are not harvested, but instead decay by releasing heat. The efficiency of the above-mentioned processes strongly depends on the size, shape, and composition of the PNPs. These dependencies need to be studied independently in order to reveal the true potential of the HEI mechanism. Of particular importance is the PNP composition, since it not only affects the metal/semiconductor Schottky energy barrier[8] but also determines the plasmon-induced hot electron energies.

Recent theoretical studies[8−12] show that the energy profile of the plasmon-induced hot electrons is extremely sensitive to the composition of the particle, which determines the amount of hot electrons that can cross the Schottky energy barrier (process ii). These studies find that intraband excitations (e.g., within the conduction band) induced by visible light can produce high-energy hot electrons and holes, while visible-light-induced interband excitations (e.g., from the d band to unoccupied states above the Fermi level) produce high-energy holes but low-energy electrons (~Fermi energy). Two metals that have been used extensively as PNPs are Ag and Au. Figure 1A illustrates that when Ag is illuminated with visible light, only intraband transitions occur, generating highly energetic hot electrons. In contrast to this, Figure 1B illustrates that when Au is illuminated with visible light, interband transitions occur due to its relatively lower interband energy (~2.3 eV), resulting in the generation of hot electrons with low energies.[12] Therefore, the visible-light-induced interband transitions limit the production of highly energetic electrons in Au, making it a less attractive hot electron injector material than Ag for solar-driven applications. However, small light-absorbing Ag PNPs exhibit resonance frequencies in the violet region of the visible spectrum, overlapping with the absorption of most promising metal oxides. Ideally, the PNP absorption should be tuned to absorb light with energies below the metal oxide band gap to extend the light absorption of the semiconductor. One promising way to red-shift the resonance frequency of Ag PNPs in a controlled way is by alloying the Ag nanoparticles with Au.[13] Since the resonance frequency of Ag/Au nanoparticles depends on its composition, the resonance frequency can be tuned to a predefined region of the spectrum that accurately extends the light absorption of a specific semiconductor. However, while significant attention has been given to study the hot electron energy and the hot electron injection ability of pure metal PNPs,[8−12] the hot electron energies and injection efficiencies of alloy PNPs are still unknown. This work experimentally explores the HEI ability of Ag/Au alloy PNPs to increase the PEC efficiency of TiO_2 photoanodes. Moreover,

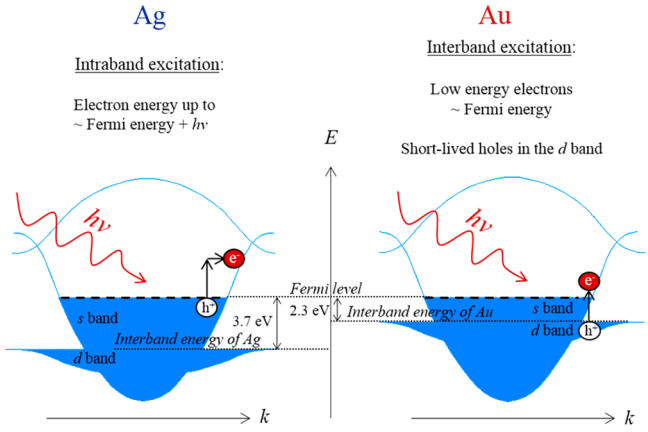

Figure 1. Illustration of the phonon-assisted intraband electronic transitions in Ag PNPs (A) and interband electronic transition in Au PNPs (B) when illuminated with visible light. Specifically, interband transitions in Au are caused by violet, blue, and green light in the visible spectrum, which have higher energies than the interband energy threshold of Au. Phonon-assisted intraband transition (A) is given here as an example; however, other competing processes can also assist intraband transitions, such as direct absorption (for PNPs smaller than ~10 nm) or electron−electron scattering (prominent for light with shorter wavelengths within the visible range). Only phonon-assisted and direct intraband transitions result in energetic hot electrons.[14]

we compare the HEI efficiencies of the alloy PNPs with their pure metal counterparts (Ag and Au PNPs) by using PNPs of the same shape and size.

RESULTS AND DISCUSSION

Ag, Au, and Ag/Au alloy PNPs were produced in the gas phase with a spark discharge particle generator,[15] where high-frequency electrical discharges are induced between two closely spaced metal rods of the corresponding metals (i.e., Au, Ag, and 50−50 atomic % Au/Ag alloy). The metallic vapor produced in each electrical discharge is dragged with a nitrogen gas flow, where the vapor condensates into nanoparticles,[16] which subsequently agglomerate to form larger fractals. These fractal particles were then made spherical by passing them through an oven and size selected to 15 nm with a differential mobility analyzer.[17] The round morphology and size (i.e., 15 nm) of the synthesized PNPs are confirmed with transmission electron microscopy (TEM) as shown in Figure 2.

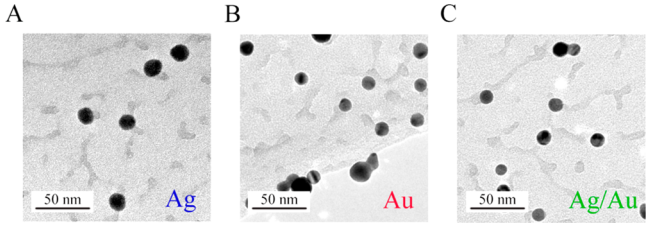

Figure 2. TEM micrographs of the synthesized Ag (A), Au (B), and alloy (C) PNPs.

In order to study the effect of the synthesized PNPs on the PEC properties of TiO_2, the PNPs of the three compositions were deposited from the gas phase onto the surface of ultrathin TiO_2 films. Three-electrode PEC measurements were carried out in a water/methanol solution. In these experiments the methanol acts as a sacrificial agent, removing the (i)

DOI: 10.1021/acsphotonics.6b01048
ACS Photonics 2017, 4, 1146−1152

photogenerated holes (due to TiO_2 interband excitations) that reach the surface of the semiconductor and the (ii) plasmon-induced "hot" holes generated in the PNPs. The most likely reactions to occur on the photoanode are the oxidation of methanol to formaldehyde and, to a lesser extent, further oxidation of formaldehyde to formate. On the other hand, the corresponding electrons migrate to a Pt counter electrode to drive the hydrogen evolution reaction.

Cyclic voltammetry measurements under solar illumination for the bare TiO_2 sample and the PNP-decorated samples are shown in Figure 3. In the anodic sweep of the Ag PNP-

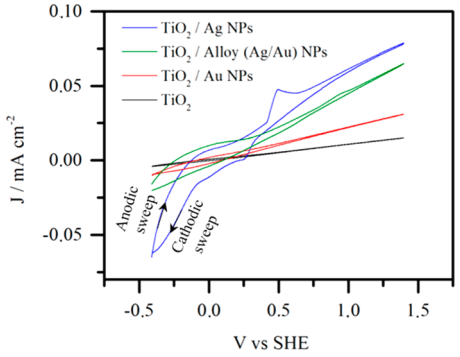

Figure 3. Anodic and cathodic cyclic voltammetry sweeps under solar illumination for the TiO_2 films with and without decorating PNPs. The corresponding cyclic voltammetry sweeps in the dark are shown in Figure S1 (Supporting Information).

decorated sample, a Ag oxidation peak can be clearly seen at ~0.5 V vs SHE, which limits the plasmonic effects of Ag PNPs to devices that operate at lower applied potentials (<0.5 V vs SHE). In the cathodic sweep the corresponding reduction peak can be seen at ~0.25 V vs SHE. In the anodic sweep of the sample decorated with alloy PNPs, the oxidation peak exhibits an anodic shift with respect to that of the Ag sample (cf. Figure 3). Therefore, alloying Ag with Au extends the stability of Ag to a larger range of applied potentials. On the other hand, the sample decorated with Au PNPs does not present an oxidation peak at the applied potentials.

At applied potentials below the beginning of the oxidation peak of the corresponding decorating metal PNPs (below ~0.5 V vs SHE for Ag, below ~0.8 V vs SHE for Ag/Au, and the full measured range for Au), a clear enhancement on the photocurrent density can be observed for all the decorated samples when compared with the bare TiO_2 sample. The origin of this photocurrent density enhancement can be a contribution of optical and electrochemical PNP effects acting below and above the semiconductor's OBGE. The wavelength-dependent incident photon to current efficiency (IPCE) of the bare TiO_2 film is shown in Figure 4, together with the IPCE of a TiO_2 film decorated with Ag PNPs. The bare TiO_2 sample exhibits a photocurrent response only below 380 nm, which is consistent with its OBGE energy. On the other hand, the sample decorated with Ag PNPs not only increased the performance of the bare semiconductor above its OBGE (i.e., below ~380 nm) but also extended the photoresponse of the semiconductor device to the visible region of the spectrum (from 380 to 540 nm), below the semiconductor OBGE energy. The photocurrent enhancement above the OBGE could be due to (i) a plasmonic effect (e.g., photonic enhancement[18]), (ii) a surface effect that facilitates the charge transfer

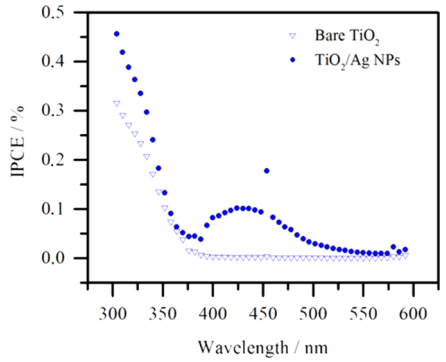

Figure 4. IPCE values of a TiO_2 film with and without decorating 15 nm Ag PNPs at −0.1 V vs SHE.

from the surface to the electrolyte (e.g., improved catalysis[19]), or a contribution from both (i) and (ii). On the other hand, the enhancement below the OBGE of TiO_2 can be explained only by plasmonic effects, such as the HEI mechanism,[7] by the PIRET mechanism,[6] or by a contribution of both. Therefore, we discuss both possible enhancements (i.e., below and above the OBGE) separately in the following two subsections for samples decorated with Ag, Au, and alloy (Ag/Au) PNPs.

Enhancement below the TiO_2 Optical Band Edge Energies. Figure 5A shows the IPCE increase (ΔIPCE) in the

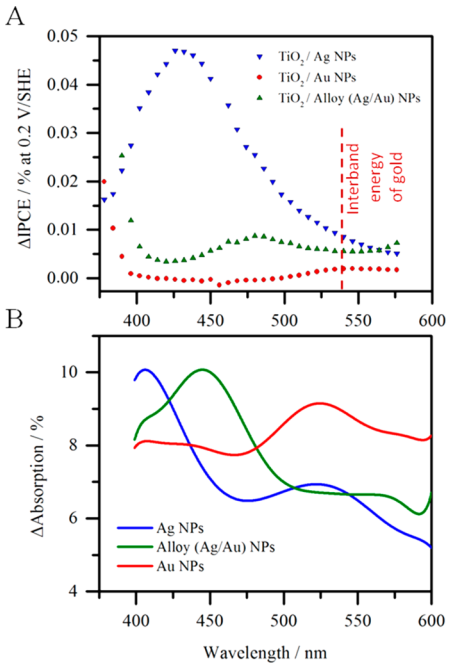

Figure 5. (A) IPCE enhancement of TiO_2 films when decorated with 15 nm Ag, alloy (Ag/Au), and Au PNPs at 0.2 V vs SHE. (B) Corresponding absorption increase.

visible region of the spectrum for TiO_2 films after decoration with either Ag, Au, or alloy (Ag/Au) PNPs. Figure 5B shows the corresponding absorption increase of the samples after the PNP deposition, which shows the surface plasmon resonance modes of the PNPs at ~405 nm for Ag, ~525 nm for Au, and ~450 nm for the alloy, which are in good agreement with other studies on alloy (Ag/Au) PNPs.[20] Clearly, the IPCE values increased upon PNP deposition in distinct regions of the spectrum that correspond to the surface plasmon resonance

DOI: 10.1021/acsphotonics.6b01048
ACS Photonics 2017, 4, 1146−1152

mode of each PNP material. It is observed, however, that the IPCE peaks are red-shifted (by ~25 nm) with respect to the absorption peaks, which is explained by the change in the PNP surrounding media refractive indexes used in the absorption (air) and IPCE (water/methanol solution) measurements.[21] The IPCE enhancement for each of the materials tested exhibited an almost symmetrical shape with a mode at the corresponding surface plasmon resonance frequencies. If PIRET would be playing a major role in the enhancement, the IPCE increase (ΔIPCE) curve would be proportional not only to the surface plasmon resonance curve but also to the TiO_2 absorption bands, which increases with decreasing wavelength. Instead, the enhancements in Figure 5A are only proportional to the surface plasmon resonance absorption modes, and, therefore, it can be concluded that the HEI mechanism, which is independent of the semiconductor absorption, is the most prominent contributor to the enhancements. Therefore, the IPCE values below the TiO_2 band gap are proportional to the Fowler theory modified by the plasmon absorption spectrum (cf. eq 1)[22,23] that predicts the number of hot electrons with sufficient energy to overcome the metal/semiconductor energy barrier:

$$\mathrm{IPCE} \approx C_F \frac{(h\nu - q\phi_B)^2}{h\nu} S(\nu) \quad (1)$$

where C_F is the Fowler emission coefficient, $h\nu$ is the energy of the excitation light, $q\phi_B$ is the metal/semiconductor interfacial energy barrier, and $S(\nu)$ is the plasmon absorption spectrum.

Even though each of the TiO_2 samples decorated with PNPs of different compositions (i.e., Ag, Au, and Ag/Au) increased their visible light absorption by ~10% at the PNPs' resonance frequencies (Figure 5B), the corresponding IPCE increase differed significantly (cf. Figure 5A). Namely, Ag exhibited an IPCE increase of ~0.05% at ~430 nm, while the alloy exhibited an increase of ~0.01% and Au an increase of less than 0.01% at their corresponding resonance frequencies. If the IPCE values in Figure 5A would be limited by light absorption, each of the PNPs with different compositions (Ag, Au, and alloy) should exhibit the highest IPCE values at their corresponding resonance frequencies, where they absorb the most light (generating the largest hot electron populations). However, the Ag PNPs' IPCE increase is larger than that for the Au and alloy PNPs throughout the measured spectrum (cf. Figure 5A). At the resonance frequency of the alloy PNPs (i.e., ~475 nm) and the resonance frequency of the Au PNPs (~550 nm), where the Ag PNPs absorb less light than its counterparts, Ag exhibits larger IPCE values. Therefore, the IPCE values of the alloy and Au PNPs in Figure 5A must not be limited by a low population of plasmon-induced hot electrons (light absorption, $S(\nu)$ in eq 1) but, instead, by a nonefficient hot electron injection process. A plausible explanation for the low HEI efficiency of Au is that above its interband energy of ~2.3 eV (below ~539 nm) hot electrons are mainly created by interband excitations and have low energies (~Fermi energy) as explained above (cf. Figure 1). Therefore, Au hot electrons generated by light energies below ~539 nm do not surpass the interface energy barrier, and, thus, no photocurrent is produced in this range (red data points in Figure 5A). More interestingly, the alloy PNPs, unlike the Au PNPs, exhibit an IPCE response below ~539 nm (above the interband energy of Au), which suggests that the alloy PNPs' interband energy threshold is shifted to lower wavelengths, allowing energetic intraband-induced hot electrons to cross the interfacial energy barrier. The interband energy threshold of the Ag/Au alloy is expected to be located around 3 eV (~413 nm), between that of Ag (~3.7 eV) and that of Au (~2.3 eV).[24] However, unlike the pure metals, the Ag/Au alloy does not exhibit a sharp threshold energy of interband transition,[24] and its hot electron energies have not been predicted or studied. The interband transition threshold energies of the synthesized PNPs are studied here by X-ray photoelectron spectroscopy (XPS) in order to investigate the origin (i.e., interband or intraband) of the generated hot electrons. The valence band XPS spectra of the Ag, Au, and alloy PNPs are shown in Figure 6. The sharp intensity increase

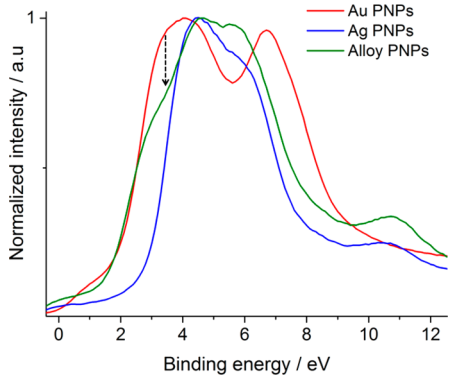

Figure 6. Valence band XPS spectra of the synthesized PNPs.

in the XPS spectra of Ag and Au correspond to their d-band energies (with respect to the Fermi level of the metal), which are in good agreement with the optical interband energy thresholds of the pure metals (~2.3 eV for Au and 3.7 eV for Ag). Unlike the pure metallic PNPs, the alloy PNPs exhibit a valence band spectrum without a sharp intensity increase, and, therefore, a distinct interband energy threshold cannot be assigned to them. Instead of a sharp transition, the alloy d-band density of states increases progressively (Figure 6) from ~2.3 eV (interband energy threshold of Au) to ~3.7 (interband energy threshold of Ag). Within this transition energy region the alloy is expected to generate less visible-light-induced interband excitations than Au due to the decrease in the d-band density of states revealed by the XPS spectra (cf. dashed arrow in Figure 6). A decrease in interband excitations increases the probability of intraband excitations (generation of energetic hot electrons), which can explain the visible light HEI response between ~450 and ~520 nm of the alloy PNPs (green data points in Figure 5A). Nevertheless, even though the XPS spectrum of alloy PNPs exhibits a more limited d-band density of states than Au in the visible region energy, only the Ag PNPs with a well-defined threshold energy of ~3.7 eV ensure that only intraband transitions are generated in the visible region. Therefore, while in the alloy PNPs a fraction of the hot electrons is generated by interband excitations and does not cross the interfacial barrier due to their low energy (~Fermi energy), in Ag PNPs only energetic intraband hot electrons are created, resulting in larger HEI efficiencies (Figure 5A). Figure 7 illustrates the relation between the d-band energy with respect to the metal Fermi level (revealed by XPS, Figure 6) and the efficiency of the HEI process (Figure 5A), which explains the decrease in HEI efficiencies with increasing Au composition in the tested PNPs.

DOI: 10.1021/acsphotonics.6b01048
ACS Photonics 2017, 4, 1146−1152

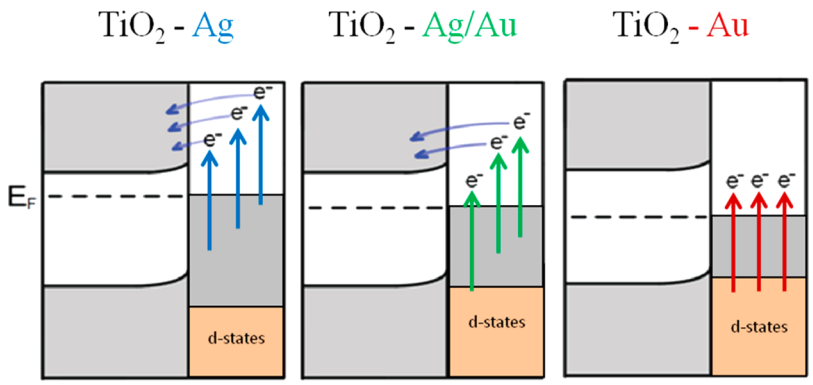

Figure 7. Illustration of the relative Fermi equilibration energies (E_f) and hot electron energy (above the Fermi level equilibration) of Ag, alloy (Ag/Au), and Au PNPs when illuminated with visible light. When Ag is illuminated, only intraband transitions occur, since the energy difference between the position of the d-states and the Fermi level is larger than that of the irradiating visible light. On the other hand, Au allows for prominent interband excitations when illuminated with violet, blue, and green light, due to its relatively shorter distance between the d-states and Fermi level. When Ag/Au is illuminated, it undergoes less interband excitations than Au, since its d-states are shifted further away from the Femi level. Interband excitations exhibit low hot electron energies (~Fermi energy), limiting the HEI process.

Moreover, the energetic intraband hot electrons in the alloy PNPs are also expected to have a lower HEI efficiency than those generated in the Ag PNPs, due to the higher interfacial energy at the alloy/TiO_2 interface when compared to that of Ag/TiO_2. According to the Schottky–Mott rule, the interfacial energy barrier can be estimated by the difference between the work function of the metal (~4.26 eV for Ag and ~5.1 eV for Au)[25] and the electron affinity of the semiconductor (~3.9 eV for TiO_2).[26] Therefore, it is expected that the interfacial energy barrier of the alloy/semiconductor interface will increase with increasing Au composition due to the larger work function of Au when compared to Ag. Such an increase in the interfacial barrier with increasing Au composition would decrease the HEI efficiency (cf. eq 1) of the energetic intraband hot electrons.

Another material-dependent process that can affect the HEI efficiencies is the hot electron charge transport from the excitation point to the extraction point (i.e., PNP/semiconductor interface). However, the average intraband charge carrier mean free paths are expected to be ~20 nm for both Au and Ag,[9,12] which is more than double the radius of the particles used in this work. These mean free path values virtually ensure that the hot carriers reach the PNP surface and can be extracted. Therefore, the differences in the hot electron energies between the PNP materials are a more plausible explanation to the material-dependent HEI efficiencies shown in Figure 5A.

In order to estimate the injection efficiency of visible-light-induced intraband hot electrons obtained in this work, the absorbed photon to current conversion efficiency (APCE) was calculated by correcting the IPCE (Figure 5A) for the absorbed light (Figure 5B). Ag PNPs exhibited an APCE of ~0.5% when illuminated with 425 nm light. Therefore, while this work clearly shows that visible-light-induced intraband hot carriers can be extracted more efficiently than interband hot carriers, the intraband HEI efficiency (~0.5%) of the tested 15 nm Ag PNPs has been proven to be too limited for any solar-to-fuel energy conversion application. The low efficiency indicates that most of the visible light energy absorbed by the 15 nm Ag PNPs is dissipated thermally.

Enhancement above the TiO_2 Optical Band Edge. Figure 8 shows the TiO_2 IPCE enhancements upon deposition of Ag (Figure 8A), Au (Figure 8B), and alloy (Figure 8C) PNPs for five different applied potentials (namely, −0.1, 0.2, 0.5, 0.8, and 1.1 V vs SHE). While increasing the applied potential does not significantly change the enhancement below the OBGE, the enhancement above the OBGE increases progressively. In addition, the enhancement above the OBGE is orders of magnitude larger than that of the HEI below the OBGE, which indicates that any contribution from the HEI mechanism above the OBGE is not significant compared to

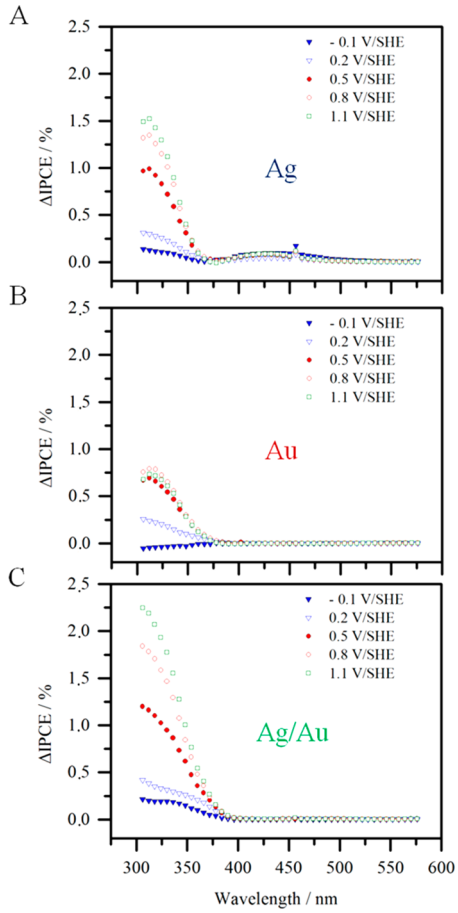

Figure 8. Wavelength-dependent IPCE enhancement curve of TiO_2 films when decorated with 15 nm Ag (A), Au (B), and alloy (Ag/Au, C) PNPs at different applied potentials.

DOI: 10.1021/acsphotonics.6b01048
ACS Photonics 2017, 4, 1146–1152

other effects. Above the OBGE, light-trapping mechanisms such as light concentration and light scattering can play an important role. However, the extinction of light by the small PNPs used in this study is primarily due to light absorption and not due to light scattering. Therefore, in our experiments, light trapping due to the concentration of light around the decorating PNPs is the only relevant mechanism that could play a role in the measured enhancement. However, light-trapping mechanisms occur only in the region of the spectrum where the absorption of the PNP and the absorption of the semiconductor overlap. According to this interpretation, the sample decorated with Ag PNPs should exhibit the most pronounced light-trapping effect, since its surface plasmon resonance is positioned approximately at the TiO_2 band gap edge region and, therefore, traps light that can be absorbed by the semiconductor. On the other hand, the samples decorated with Au and alloy PNPs exhibit a surface plasmon resonance at longer wavelengths, trapping light below the OBGE of the semiconductor. Clearly, the enhancement above the OBGE shown in Figure 8 is more significant for the alloy than for the pure metals (i.e., Ag and Au), which suggests that the light-trapping mechanism is not the most prominent contributor to the measured enhancement. Moreover, this lack of correlation between the PNP/semiconductor absorption overlap and the IPCE enhancement suggests that the enhancement above the OBGE is not due to any plasmonic effect but, instead, due to a cocatalytic property of the metallic PNP that facilitates the charge transfer from the semiconductor surface to the electrolyte. In order to unravel the origin of this cocatalytic effect, more electrochemical experiments (e.g., electrochemical impedance spectroscopy measurements) must be carried out.

In summary, hot electron injection efficiencies from Ag/Au alloy PNPs to TiO_2 photoanodes were compared to those of Ag and Au PNPs by measuring the photoelectrochemical conversion efficiencies of the composite photoanode below the TiO_2 OBGE. Our results revealed that Ag/Au alloy PNPs exhibit higher efficiencies than Au and significantly lower efficiencies than Ag (by ~8-fold). Since the PNPs used in this work are smaller than the mean free path of the hot electrons, the measured hot electron injection efficiencies are not limited by hot charge transport to the PNP surface. Instead, the measured hot electron injection efficiencies are expected to be limited by low hot electron energies and high interfacial energy barriers between the TiO_2 and the different metals. It is well known that Au PNPs undergo interband electronic transitions when illuminated with visible light, which results in low-energy hot electrons and, therefore, low hot electron injection efficiencies. In this work, we assign the higher hot electron injection efficiency of the Ag/Au (when compared to Au) to a decrease in visible-light-induced interband transitions. Au presents an interband energy threshold shift to higher energies (lower wavelengths) when alloyed with Ag. This shift increases the visible-light-induced intraband excitations, which results in higher hot electron energies and injection efficiencies. However, unlike the pure PNPs, the threshold energy of the alloy PNPs is not sharp and the d-band density of the states decreases progressively in a transition region. Therefore, we conclude that alloying Ag with Au decreases the interband excitations in the visible region, but does not suppress them entirely. This interband transition region was revealed here by XPS and explains the lower HEI efficiencies of the alloy PNPs when compared to the Ag PNPs. Nevertheless, the Ag/Au PNPs not only exhibit higher hot electron injection efficiencies than Au but, unlike their pure counterparts, also allow tuning their absorption spectrum by changing their Ag/Au composition ratio. Such tunability can be used to perfectly extend the light utilization of semiconductors to lower light energies (<OBGE).

Despite the advantages in stability and absorption tunability of PNPs, the HEI efficiencies measured in this work (e.g., APCE of ~0.5% for 15 nm Ag PNPs at 425 nm) are too low for any photoelectrochemical solar-to-fuel energy conversion applications (e.g., water splitting, CO_2 reduction). From the measured efficiencies we conclude that most of the absorbed visible light in 15 nm Ag, Au, and alloy (Ag/Au) PNPs dissipates without generating energetic hot electrons.

Finally, the photoelectrochemical conversion efficiency of the TiO_2 film was also studied by irradiating light with energies above the semiconductor's OBGE. In this region of the spectrum (λ < ~380 nm), the photocurrent of the PNP/TiO_2 composites is mainly due to TiO_2 interband excitations. When the metal PNPs were deposited, the IPCE of the semiconductor significantly increased. This increase cannot be caused by light-trapping effects due to the lack of absorption overlap between the PNPs and the semiconductor. Instead, the photocurrent increase is ascribed here to a more efficient charge transfer across the semiconductor electrolyte interface upon the metallic PNP deposition. However, the origin of this charge transport effect must be further investigated.

METHODS

PNP Synthesis. The 15 nm Ag, Au, and Ag/Au PNPs were synthesized in the gas phase with a spark discharge particle generator coupled with a differential mobility analyzer as described briefly above and in detail elsewhere.[27] In the spark discharge particle generator electrodes of Ag, Au, and Ag/Au alloy (50−50 atomic %) were used for the PNP synthesis of the corresponding compositions. The electrodes, having a purity of 99.95%, were purchased from Goodfellow Cambridge Limited.

TiO_2/Metallic PNP Composite Electrode Synthesis. A 10 nm film of Ti was deposited on FTO (fluorine tin oxide)-coated glass substrates by magnetron sputter deposition. The samples were annealed in a tube oven at 500 °C for 5 h under flowing air (20 mL/min) to oxidize the Ti films to TiO_2. Charged metallic PNPs were deposited electrostatically from the gas phase to the TiO_2 surface.

Photoelectrochemical Measurements. The photoelectrochemical measurements (shown in Figures 3, 4, 5A, 8, and S1) were carried out in a methanol/water (50 v/v %) solution in an electrochemical cell using a three-electrode configuration: a working electrode whose potential was controlled by a potentiostat (EG&G PAR 283), a reference Ag/AgCl electrode (XR300, saturated KCl + AgCl solution (KS120), Radiometer Analytical), and a coiled Pt wire as a counter electrode. The photocurrent measurements shown in Figures 3 and S1 were performed under simulated AM1.5 solar illumination with a Newport Sol3A Class AAA solar simulator (type 94023A-SR3). The monochromatic photocurrents (IPCE) shown in Figures 4, 5A, and 8 were measured using a 200 W quartz tungsten−halogen lamp coupled into a grating monochromator with a 6 nm step, as described in detail elsewhere.[28]

Absorption Measurements. The absorption spectra measurements of the PNPs shown in Figure 5B were carried out with a PerkinElmer-Lambda 900 spectrometer equipped with an integrated sphere device. Measurements were conducted before and after PNP deposition, so that the

DOI: 10.1021/acsphotonics.6b01048
ACS Photonics 2017, 4, 1146−1152

influence of the PNPs on the TiO_2 absorption spectra could be determined.

■ ASSOCIATED CONTENT

Supporting Information

The Supporting Information is available free of charge on the ACS Publications website at DOI: 10.1021/acsphotonics.6b01048.

Cyclic voltammetry sweeps in the dark under the same conditions as Figure 3; stability measurement (photocurrent vs time) of Ag PNPs when illuminated with visible light (PDF)

■ AUTHOR INFORMATION

Corresponding Authors

*E-mail: m.valenti@tudelft.nl.
*E-mail: w.smith@tudelft.nl.

ORCID

Marco Valenti: 0000-0002-0403-182X
Wilson A. Smith: 0000-0001-7757-5281

Notes

The authors declare no competing financial interest.

■ ACKNOWLEDGMENTS

This work is supported by an NWO VIDI grant awarded to W.A.S. We thank Nejra Causevic for making the table of contents image, Joost Middelkoop for the TEM measurements, Herman Schreuders for the magnetron sputter deposition, and Bart Boshuizen for the XPS measurements.

■ REFERENCES

(1) Fujishima, A.; Honda, K. Electrochemical Photolysis of Water at a Semiconductor Electrode. *Nature* **1972**, *238*, 37−38.
(2) Sivula, K.; van de Krol, R. Semiconducting materials for photoelectrochemical energy conversion. *Nat. Rev. Mater.* **2016**, *1*, 15010.
(3) Mubeen, S.; Lee, J.; Singh, N.; Kramer, S.; Stucky, G. D.; Moskovits, M. An autonomous photosynthetic device in which all charge carriers derive from surface plasmons. *Nat. Nanotechnol.* **2013**, *8*, 247−251.
(4) Cushing, S. K.; Li, J.; Bright, J.; Yost, B. T.; Zheng, P.; Bristow, A. D.; Wu, N. Controlling Plasmon-Induced Resonance Energy Transfer and Hot Electron Injection Processes in Metal@TiO2 Core−Shell Nanoparticles. *J. Phys. Chem. C* **2015**, *119*, 16239−16244.
(5) Mubeen, S.; Lee, J.; Liu, D.; Stucky, G. D.; Moskovits, M. Panchromatic Photoproduction of H2 with Surface Plasmons. *Nano Lett.* **2015**, *15*, 2132−2136.
(6) Cushing, S. K.; Li, J.; Meng, F.; Senty, T. R.; Suri, S.; Zhi, M.; Li, M.; Bristow, A. D.; Wu, N. Photocatalytic Activity Enhanced by Plasmonic Resonant Energy Transfer from Metal to Semiconductor. *J. Am. Chem. Soc.* **2012**, *134*, 15033−15041.
(7) Clavero, C. Plasmon-induced hot-electron generation at nanoparticle/metal-oxide interfaces for photovoltaic and photocatalytic devices. *Nat. Photonics* **2014**, *8*, 95−103.
(8) Sundararaman, R.; Narang, P.; Jermyn, A. S.; Goddard Iii, W. A.; Atwater, H. A. Theoretical predictions for hot-carrier generation from surface plasmon decay. *Nat. Commun.* **2014**, *5*, 5788.
(9) Brown, A. M.; Sundararaman, R.; Narang, P.; Goddard, W. A.; Atwater, H. A. Nonradiative Plasmon Decay and Hot Carrier Dynamics: Effects of Phonons, Surfaces, and Geometry. *ACS Nano* **2016**, *10*, 957−966.
(10) Govorov, A. O.; Zhang, H.; Gun'ko, Y. K. Theory of Photoinjection of Hot Plasmonic Carriers from Metal Nanostructures into Semiconductors and Surface Molecules. *J. Phys. Chem. C* **2013**, *117*, 16616−16631.
(11) Manjavacas, A.; Liu, J. G.; Kulkarni, V.; Nordlander, P. Plasmon-Induced Hot Carriers in Metallic Nanoparticles. *ACS Nano* **2014**, *8*, 7630−7638.
(12) Bernardi, M.; Mustafa, J.; Neaton, J. B.; Louie, S. G. Theory and computation of hot carriers generated by surface plasmon polaritons in noble metals. *Nat. Commun.* **2015**, *6*, 7044.
(13) Verbruggen, S. W.; Keulemans, M.; Martens, J. A.; Lenaerts, S. Predicting the Surface Plasmon Resonance Wavelength of Gold−Silver Alloy Nanoparticles. *J. Phys. Chem. C* **2013**, *117*, 19142−19145.
(14) Khurgin, J. B. How to deal with the loss in plasmonics and metamaterials. *Nat. Nanotechnol.* **2015**, *10*, 2−6.
(15) Schwyn, S.; Garwin, E.; Schmidtott, A. AEROSOL GENERATION BY SPARK DISCHARGE. *J. Aerosol Sci.* **1988**, *19*, 639−642.
(16) Feng, J.; Biskos, G.; Schmidt-Ott, A. Toward industrial scale synthesis of ultrapure singlet nanoparticles with controllable sizes in a continuous gas-phase process. *Sci. Rep.* **2015**, *5*, 15788.
(17) Knutson, E. O.; Whitby, K. T. Aerosol classification by electric mobility: apparatus, theory, and applications. *J. Aerosol Sci.* **1975**, *6*, 443−451.
(18) Atwater, H. A.; Polman, A. Plasmonics for improved photovoltaic devices. *Nat. Mater.* **2010**, *9*, 205−213.
(19) Haro, M.; Abargues, R.; Herraiz-Cardona, I.; Martínez-Pastor, J.; Giménez, S. Plasmonic versus catalytic effect of gold nanoparticles on mesoporous TiO2 electrodes for water splitting. *Electrochim. Acta* **2014**, *144*, 64−70.
(20) Link, S.; Wang, Z. L.; El-Sayed, M. A. Alloy Formation of Gold−Silver Nanoparticles and the Dependence of the Plasmon Absorption on Their Composition. *J. Phys. Chem. B* **1999**, *103* (18), 3529−3533.
(21) Mie, G. Articles on the optical characteristics of turbid tubes, especially colloidal metal solutions. *Ann. Phys.* **1908**, *25*, 377−445.
(22) Fowler, R. H. The Analysis of Photoelectric Sensitivity Curves for Clean Metals at Various Temperatures. *Phys. Rev.* **1931**, *38*, 45−56.
(23) Knight, M. W.; Sobhani, H.; Nordlander, P.; Halas, N. J. Photodetection with Active Optical Antennas. *Science* **2011**, *332*, 702−704.
(24) Rioux, D.; Vallières, S.; Besner, S.; Muñoz, P.; Mazur, E.; Meunier, M. An Analytic Model for the Dielectric Function of Au, Ag, and their Alloys. *Adv. Opt. Mater.* **2014**, *2*, 176−182.
(25) Michaelson, H. B. The work function of the elements and its periodicity. *J. Appl. Phys.* **1977**, *48*, 4729−4733.
(26) Rothenberger, G.; Fitzmaurice, D.; Graetzel, M. Spectroscopy of conduction band electrons in transparent metal oxide semiconductor films: optical determination of the flatband potential of colloidal titanium dioxide films. *J. Phys. Chem.* **1992**, *96*, 5983−5986.
(27) Valenti, M.; Dolat, D.; Biskos, G.; Schmidt-Ott, A.; Smith, W. A. Enhancement of the Photoelectrochemical Performance of CuWO4 Thin Films for Solar Water Splitting by Plasmonic Nanoparticle Functionalization. *J. Phys. Chem. C* **2014**, *119*, 2096.
(28) Abdi, F. F.; van de Krol, R. Nature and Light Dependence of Bulk Recombination in Co-Pi-Catalyzed BiVO4 Photoanodes. *J. Phys. Chem. C* **2012**, *116*, 9398−9404.

DOI: 10.1021/acsphotonics.6b01048
ACS Photonics 2017, 4, 1146−1152